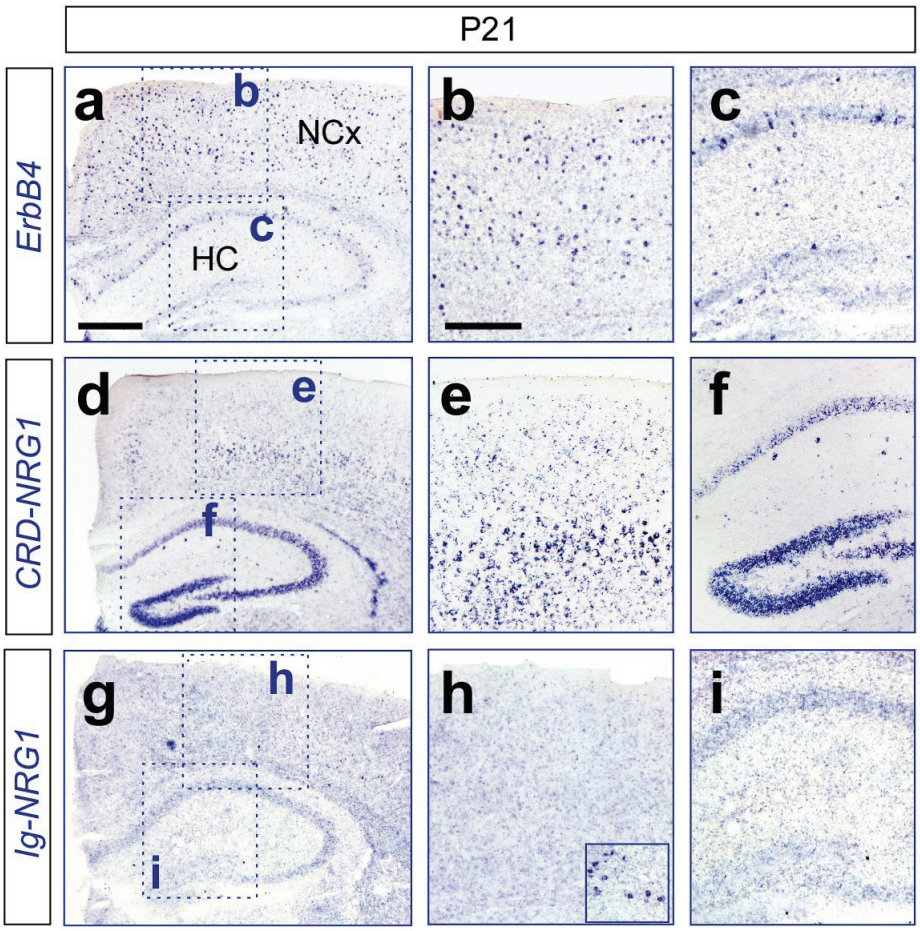

Supplementary Figure 1. *Nrg1* and *ErbB4* mRNA expression in the postnatal cortex. a-i, Coronal sections through the mouse telencephalon showing ErbB4 (a-c), CRD-Nrg1 (d-f), and Ig-Nrg1 (g-i) mRNA expression in the neocortex (NCx) and hippocampus (HC) at P21. CRD-Nrg1 and Ig-Nrg1 correspond to membrane bound (Type III) and diffusible (type I/II) products of the Nrg1 gene. The inset in (h) shows expression in diencephalic neurons from the same section. Scale bars: 500 μm (a, d, g), 300 μm (b, c, e, f, h, i).

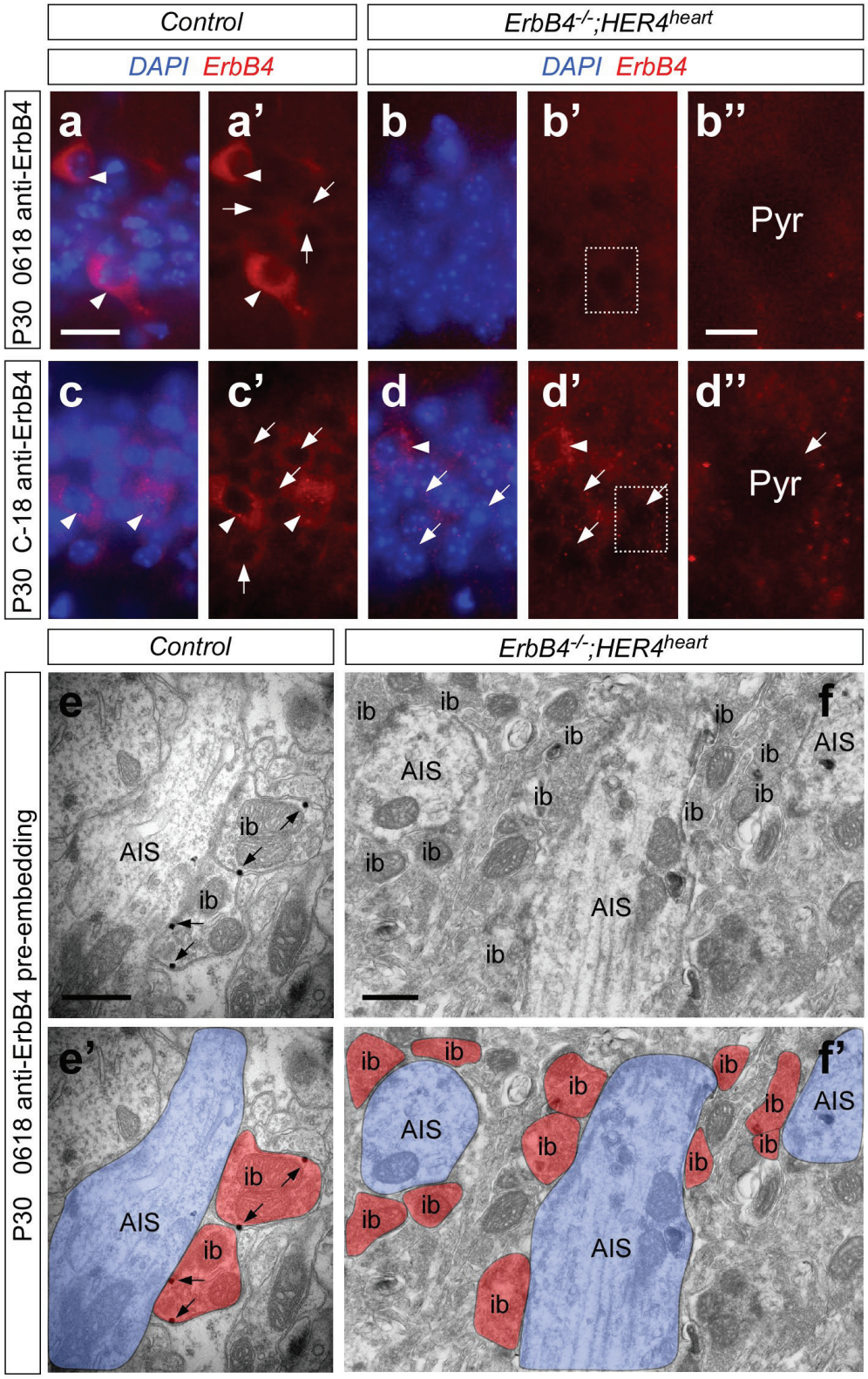

Supplementary Figure 2. Comparative analysis of ErbB4 antibody specificity. a-d'', Coronal sections through the hippocampus of P30 wild type (a, a', c, c') and *ErbB4* mutant mice (b-b'', d-d'') showing immunohistochemistry using 0618 ErbB4 (Zhu et al., EMBO J. 14, 5842-5848, 1995) (a-b'') or C-18 ErbB4 (Santa Cruz Biotechnologies, Inc.) (c-d'') antibodies. Arrowheads point to interneurons stained with ErbB4 antibodies. Note that additional staining is observed when the C-18 antibody was used. This staining persists in sections obtained from *ErbB4* mutant brains (arrows and arrowheads). **e-f'**, Pre-embedding electron microscopic localization of ErbB4 using the 0618 antibody in P30 wild type (e, e') and *ErbB4* mutant (f, f') hippocampus. Note that the immunogold labelling present in inhibitory boutons (ib) contacting the axon initial segment (AIS) of pyramidal cells in wild type animals (e, e') is completely absent in *ErbB4* mutant mice (f, f'). Scale bars: 20 μm (a, a',b, b', c, c', d, d'), 5 μm (b'', d''), 0.3 μm (e, e', f, f').

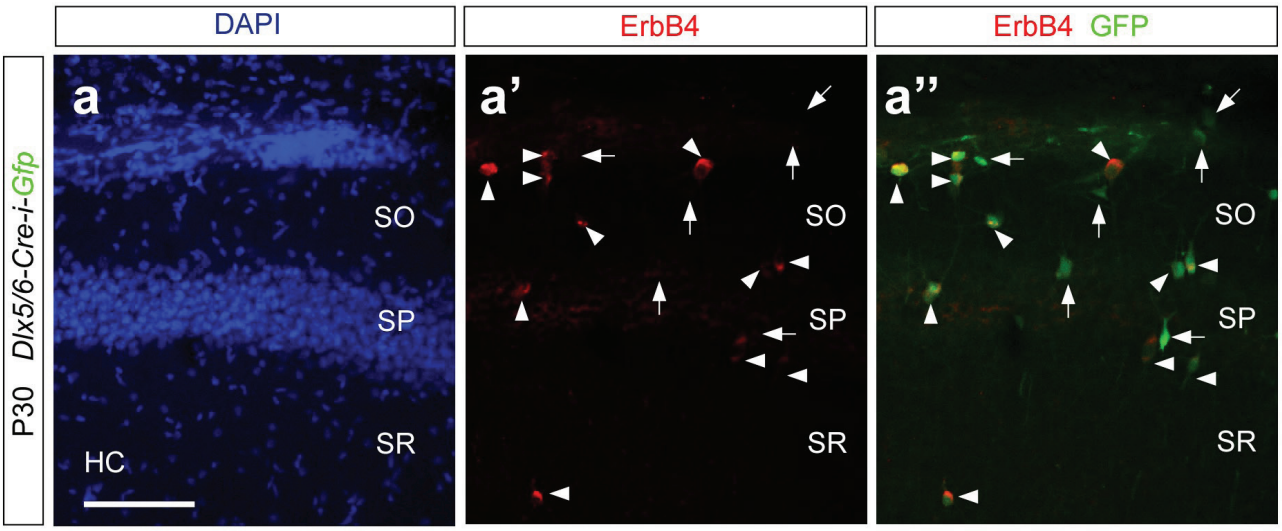

Supplementary Figure 3. Expression of ErbB4 in hippocampal interneurons. a-a'', Coronal sections through the hippocampus of a *Dlx5/6-Cre-IRES-Gfp* mouse at P30 showing immunohistochemistry against ErbB4 (full arrowheads) and GFP (arrows and full arrowheads). Virtually all ErbB4-expressing cells in the hippocampus stain for GFP (full arrowheads). HC, hippocampus; SO, stratum oriens; SP, stratum pyramidale; SR, stratum radiatum. Scale bar: 100 μm (a, a', a'').

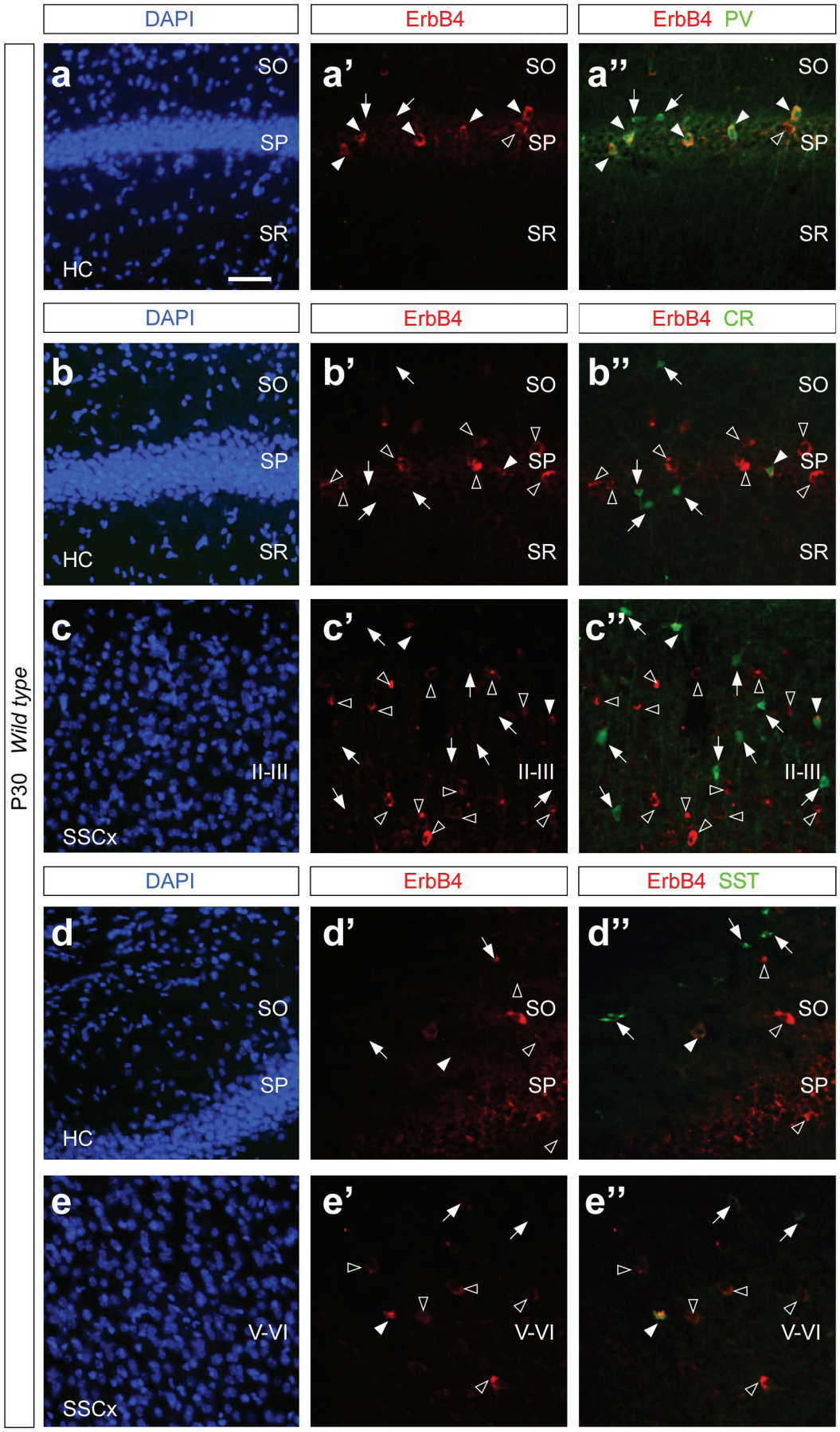

Supplementary Figure 4. Expression of ErbB4 in different classes of hippocampal interneurons. a-e'', Coronal sections through the hippocampus of a P30 mouse showing double immunohistochemistry for ErbB4 and PV (a-a''), ErbB4 and CR (b-c''), and ErbB4 and SST (d-e''). Arrowheads point to double labelled cells, open arrowheads point to ErbB4-expressing cells that do not express the other markers, and arrows point to interneurons that do not express ErbB4. HC, hippocampus; II-III, cortical layers II-III; SO, stratum oriens; SP, stratum pyramidale; SR, stratum radiatum; SSCx, somatosensory cortex; V-VI, cortical layers V-VI. Scale bar: 50 μm (a, a', a'', b, b', b'', c, c', c'', d, d', d'', e, e', e'').

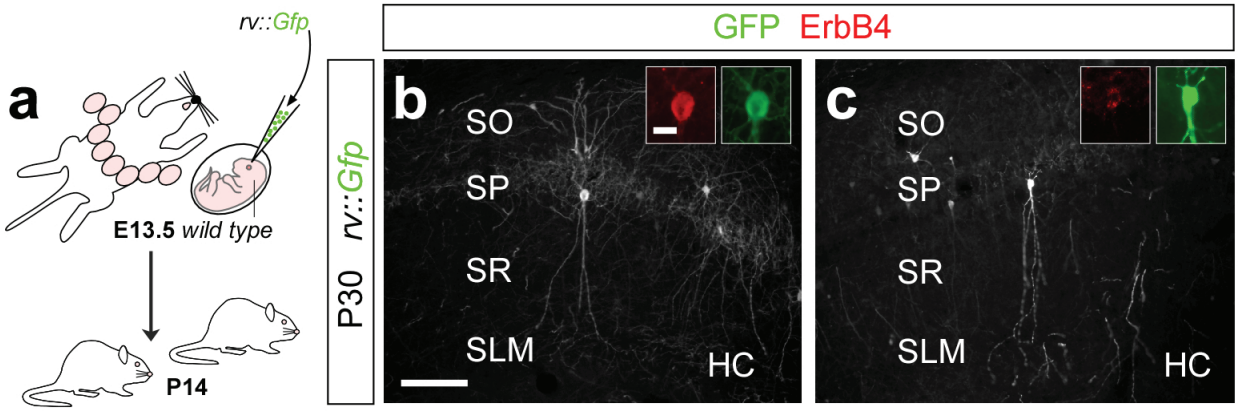

Supplementary Figure 5. Expression of ErbB4 in hippocampal basket and chandelier cells. **a**, Experimental paradigm. Retroviruses expressing Gfp (*rv::Gfp*) were injected in utero into the MGE of E13.5 wild type embryos using ultrasound guided microscopy. Transfected MGE-derived interneurons were analyzed at P14. **b, c**, Representative images of chandelier (b) and basket (c) cells in the hippocampus visualized by GFP labelling. Insets show magnification of the soma. HC, hippocampus; SO, stratum oriens; SP, stratum pyramidale; SR, stratum radiatum; SLM, stratum lacunosum moleculare. Scale bar: 100 µm.

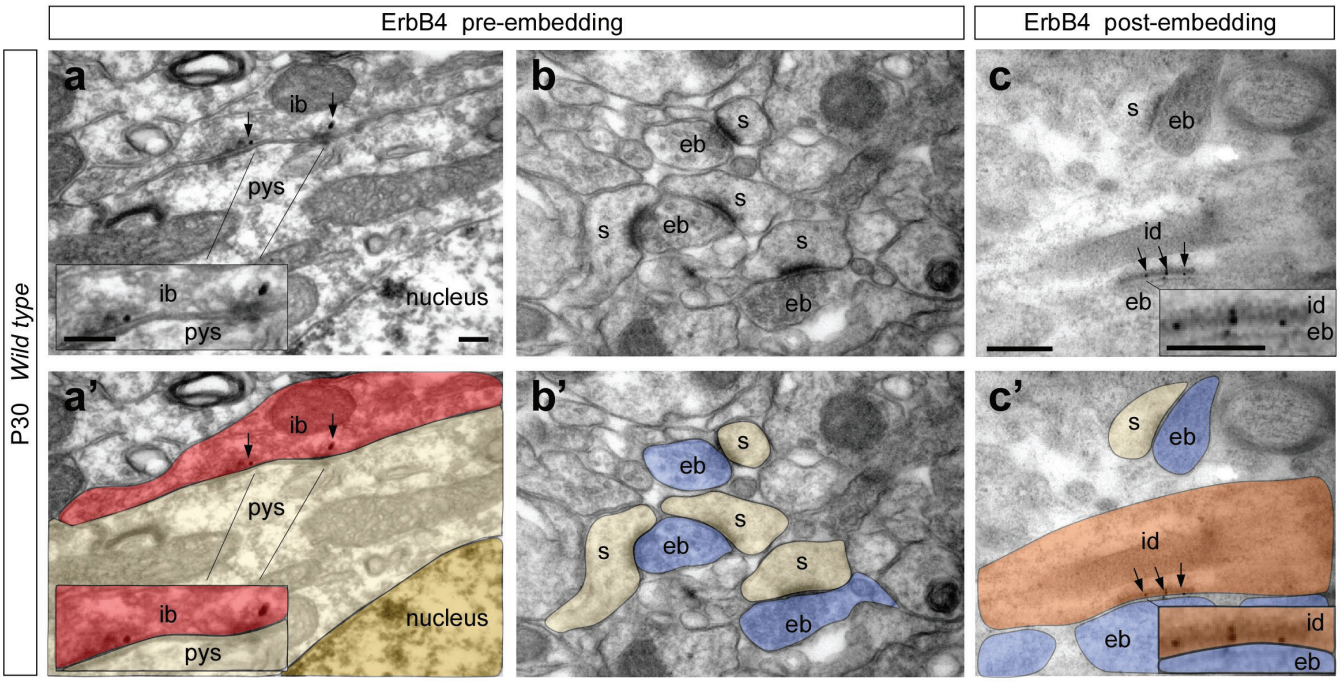

Supplementary Figure 6. Ultrastructural localization of ErbB4 in the postnatal cortex. a-c', Pre-embedding (a-b') and post-embedding (c, c') electron microscopic localization of ErbB4 in the P30 hippocampus. Immunogold labelling (arrows in a, a') localizes ErbB4 to inhibitory boutons (ib) contacting the soma of a pyramidal cell (pys). The inset shows a magnification of the inhibitory synapses. ErbB4 immunogold labelling is absent from excitatory boutons (eb) contacting the spines (s) of pyramidal cell dendrites (b-c'), while is present in the postsynaptic density of an excitatory bouton contacting the dendrite (id) of an inhibitory neuron (c, c'). The inset shows a magnification of this later synapse. Scale bars: 0.2 μm (a, a', b, b', c, c'), 0.05 μm (insets in a, c').

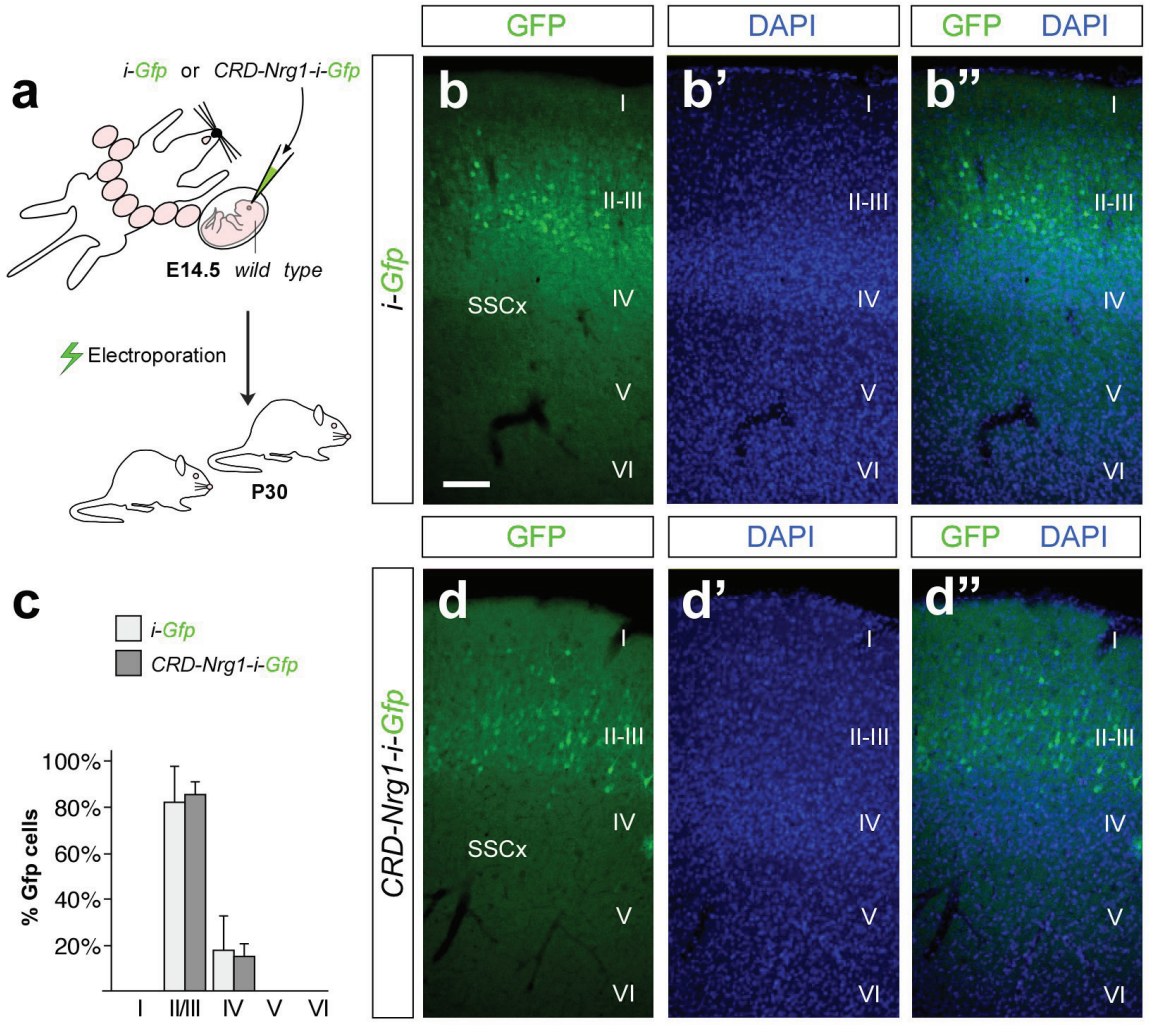

Supplementary Figure 7. *CRD-Nrg1* expression does not alter the migration of pyramidal cells. a, Experimental paradigm. Neocortical progenitor cells were electroporated in utero at E14.5 with either *Gfp* or *CRD-Nrg1-i-Gfp* plasmids, and the distribution of transfected pyramidal cells was analyzed at P30. **b-b"** and **d-d"**, Representative images showing the distribution of *Gfp* (b-b") or *CRD-Nrg1-i-Gfp*-expressing (d-d") pyramidal cells in the somatosensory cortex (SSCx). **c**, Quantification of the laminar distribution of electroporated pyramidal cells in the cortex revealed no significant differences between both experimental groups. *Gfp*: 219 neurons, from 3 brains; *CRD-Nrg1-i-Gfp*: 200 neurons, from 4 brains, P = 0.11, χ^2 test. I-VI, cortical layers I-VI. Scale bar: 100 µm.

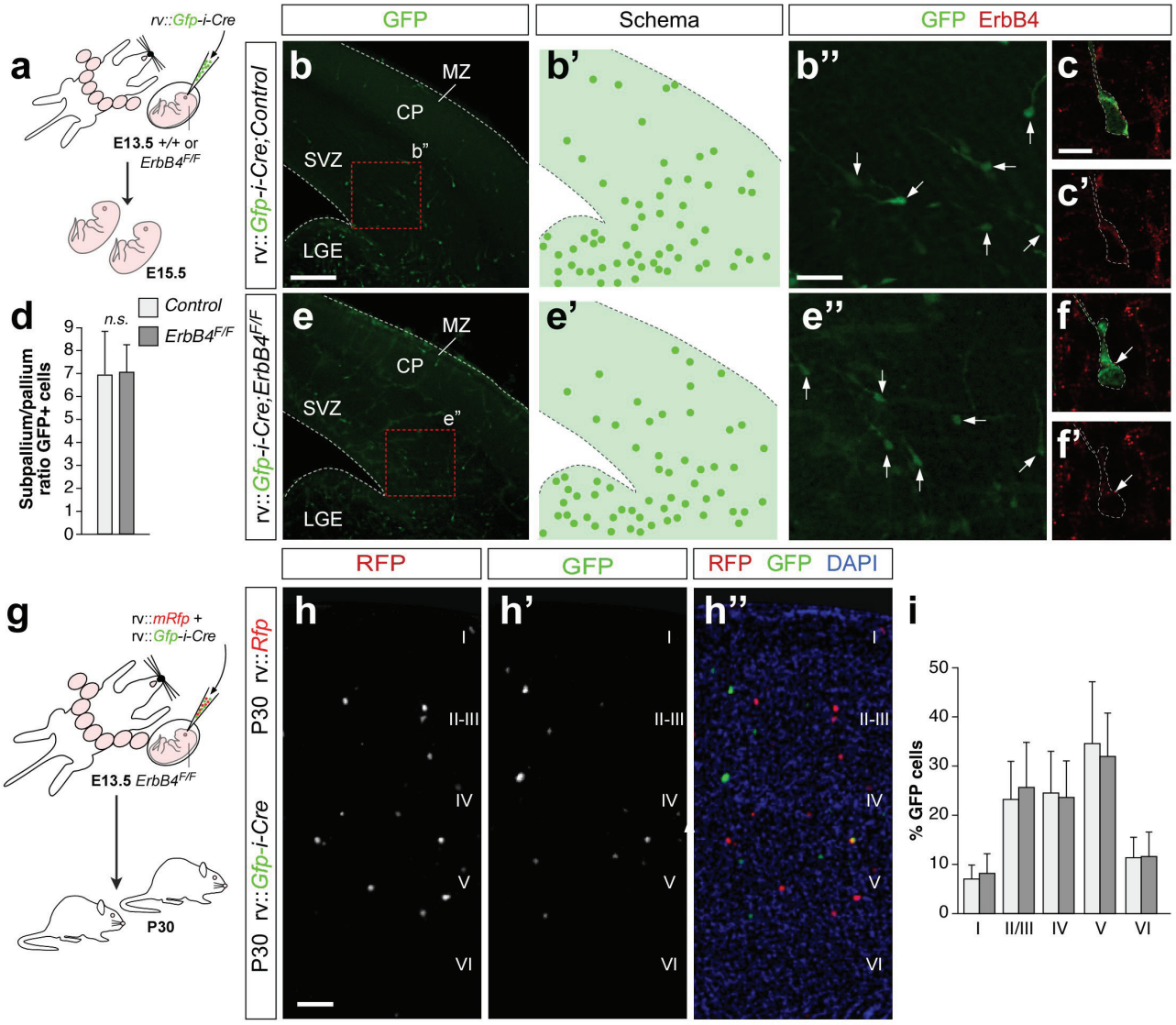

Supplementary Figure 8. Retroviral-mediated deletion of ErbB4 does not prevent interneuron migration to the cortex or laminar distribution. **a**, Experimental paradigm. Retroviruses expressing Cre and Gfp (*rv::Gfp-i-Cre*) were injected in utero into the MGE of E13.5 wild type and *ErbB4*$^{F/F}$ embryos using ultrasound guided microscopy. Transfected MGE-derived interneurons were analyzed at E15.5. **b-b"**, **e-e"**, Representative images showing the distribution of Gfp-i-Cre-expressing interneurons in control (b-b") or *ErbB4*$^{F/F}$ (e-e") embryos. The schemas depict the distribution of cells shown in (b) and (e), whereas (b") and (e") show high magnification images of the boxed areas in (b) and (e). Arrows point to migrating Gfp-i-Cre-expressing interneurons. **c, c', f, f'**, Expression of ErbB4 in Gfp-i-Cre-expressing interneurons found in the pallium of control (c, c') and *ErbB4*$^{F/F}$ (f, f') embryos. We found traces of ErbB4 in most Cre-infected interneurons located at the pallial/subpallial boundary (16 out of 20 randomly selected cells). **d**, Analysis of the subpallial/pallial ratio of GFP-expressing interneurons in control and *ErbB4*$^{F/F}$ embryos revealed no significant differences. Control: 551 neurons, 3 brains; *ErbB4*$^{F/F}$: 330 from 2 brains, P = 0.92, *t*-test. **g**, Experimental paradigm. A cocktail of retroviruses (rv) expressing either *mRfp* or *Gfp-i-Cre* was injected into the MGE of E13.5 *ErbB4*$^{F/F}$ embryos, and transfected interneurons were analyzed in the P30 cortex. **h-h"**, Laminar distribution of interneurons infected with retroviruses expressing *mRfp* (h, h") and *Gfp-i-Cre* (h', h") in the P30 cortex of *ErbB4*$^{F/F}$ mice. **i**, Quantification of the laminar distribution of mRfp and Gfp-i-Cre interneurons in the cortex revealed no significant differences between control (mRfp) and *ErbB4* mutant (Gfp-i-Cre) interneurons. Control: n = 1017; *ErbB4* mutant: n = 697 neurons, 2 brains; P = 0.74, χ^2 test. CP, cortical plate; LGE, lateral ganglionic eminence; MZ, marginal zone; SVZ, subventricular zone; I-VI, cortical layers I-VI. Scale bars: 100 μm (b, e, h-h"), 30 μm (b', e'), 10 μm (c, c', f, f').

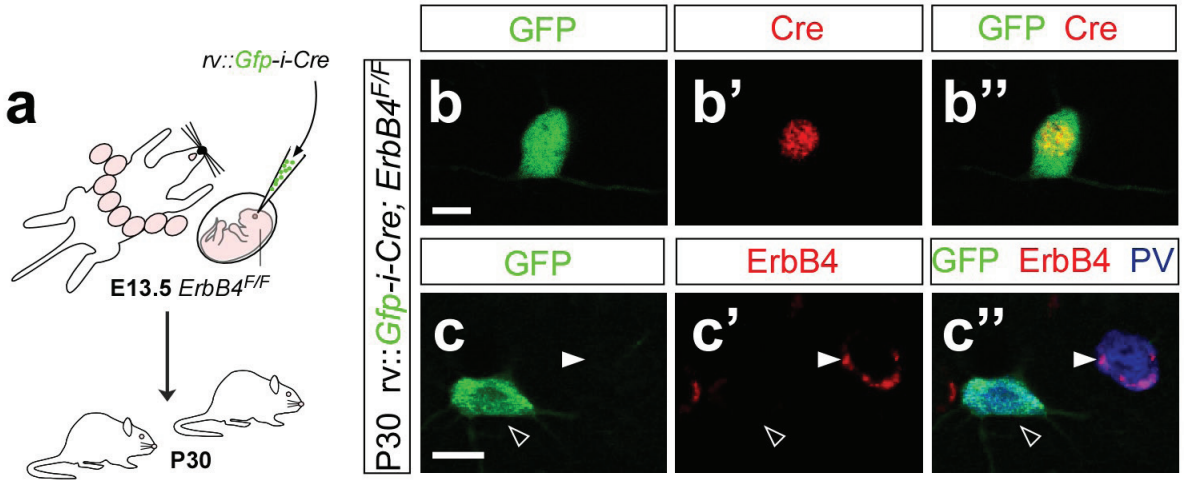

Supplementary Figure 9. Loss of ErbB4 in cortical interneurons infected with retroviruses expressing Gfp-i-Cre. **a**, Experimental paradigm. Retroviruses expressing *Cre* and *Gfp* (*rv::Gfp-i-Cre*) were injected in utero into the MGE of E13.5 *ErbB4*$^{F/F}$ embryos using ultrasound guided microscopy. Transfected MGE-derived interneurons were analyzed at P30. **b-b''**, Confocal images showing the co-expression of GFP (b, b') and Cre (b', b'') in infected cells. **c-c''**, Confocal images showing absence of ErbB4 in a PV-expressing infected interneurons (open arrowhead). Note expression of ErbB4 in another PV-expressing cell that does not contain GFP (arrowhead). Scale bars: 10 μm.

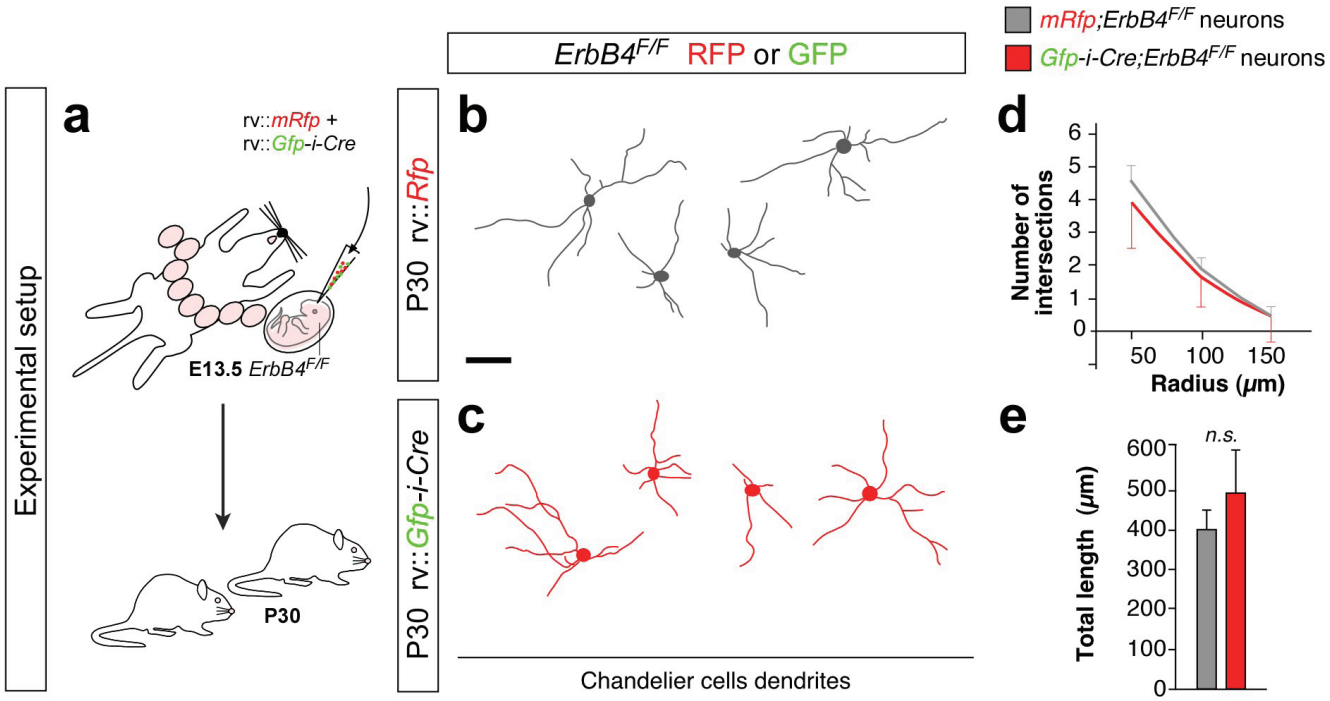

Supplementary Figure 10. Normal dendritic morphology of chandelier cells in the absence of ErbB4. **a**, Experimental paradigm. Retroviruses expressing *Cre* and *Gfp* (*rv::Gfp-i-Cre*) were injected in utero into the MGE of E13.5 *ErbB4*$^{F/F}$ embryos using ultrasound guided microscopy. Transfected MGE-derived interneurons were analyzed at P30. **b, c**, Drawings of dendritic arbours from representative wild type and *ErbB4* mutant chandelier cells. For clarity, the axon of chandelier cells is not represented in the drawings. **d, e**, Sholl analysis (P = 0.97, χ^2 test) and quantification of the total length of the dendritic arbour (P = 0.46, Welch test) revealed no differences between both experimental groups. Control: n = 9; *ErbB4* mutant: n = 9 neurons, 4 brains. Scale bar: 100 μm.

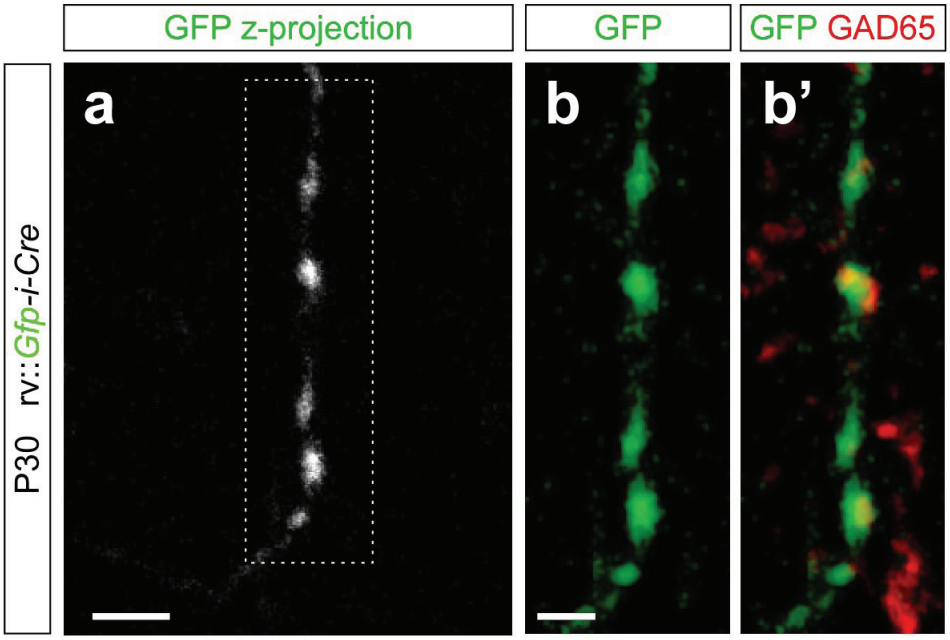

Supplementary Figure 11. GAD65 expression in axon boutons of chandelier cells candlesticks. **a**, Confocal stack projection of one axon terminal (candlestick) from a single neocortical chandelier cell at P30 labelled with GFP via embryonic retroviral infection (see Supplementary Figure 5). **b, b'**, Colocalization of GFP and GAD65 in a single confocal section of the chandelier candlestick shown in (a). GAD65 was found to be present in approximately 68% of the GFP-stained boutons (136 out of 158 GFP boutons containing GAD65 staining, 39 candlesticks). Scale bars: 2 μm (a), 1 μm (b, b').

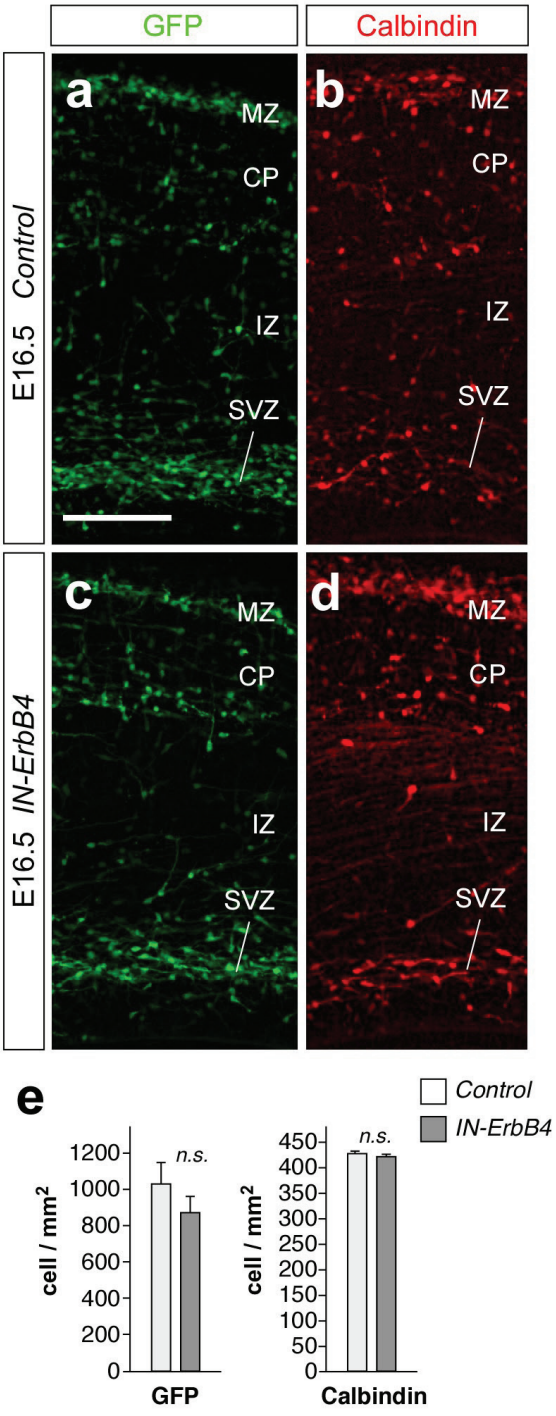

Supplementary Figure 12. Normal interneuron migration to the cortex in *IN-ErbB4* mutant embryos. a-d, Coronal sections through the pallium of E16.5 control (a, b) and *IN-ErbB4* mutant (b, d) embryos showing immunohistochemistry against GFP (from *Dlx5/6-Cre-i-Gfp*) and Calbindin (a marker of immature interneurons). **e**, Quantification of the number of GFP- and Calbindin-expressing interneurons in the pallium of E16.5 control and *IN-ErbB4* mutant embryos revealed no differences between both experimental groups. n = 3; GFP, P = 0.31, Calbindin, P = 0.20; *t*-test. CP, cortical plate; IZ, intermediate zone; MZ, marginal zone; SVZ, subventricular zone. Scale bar: 50 μm.

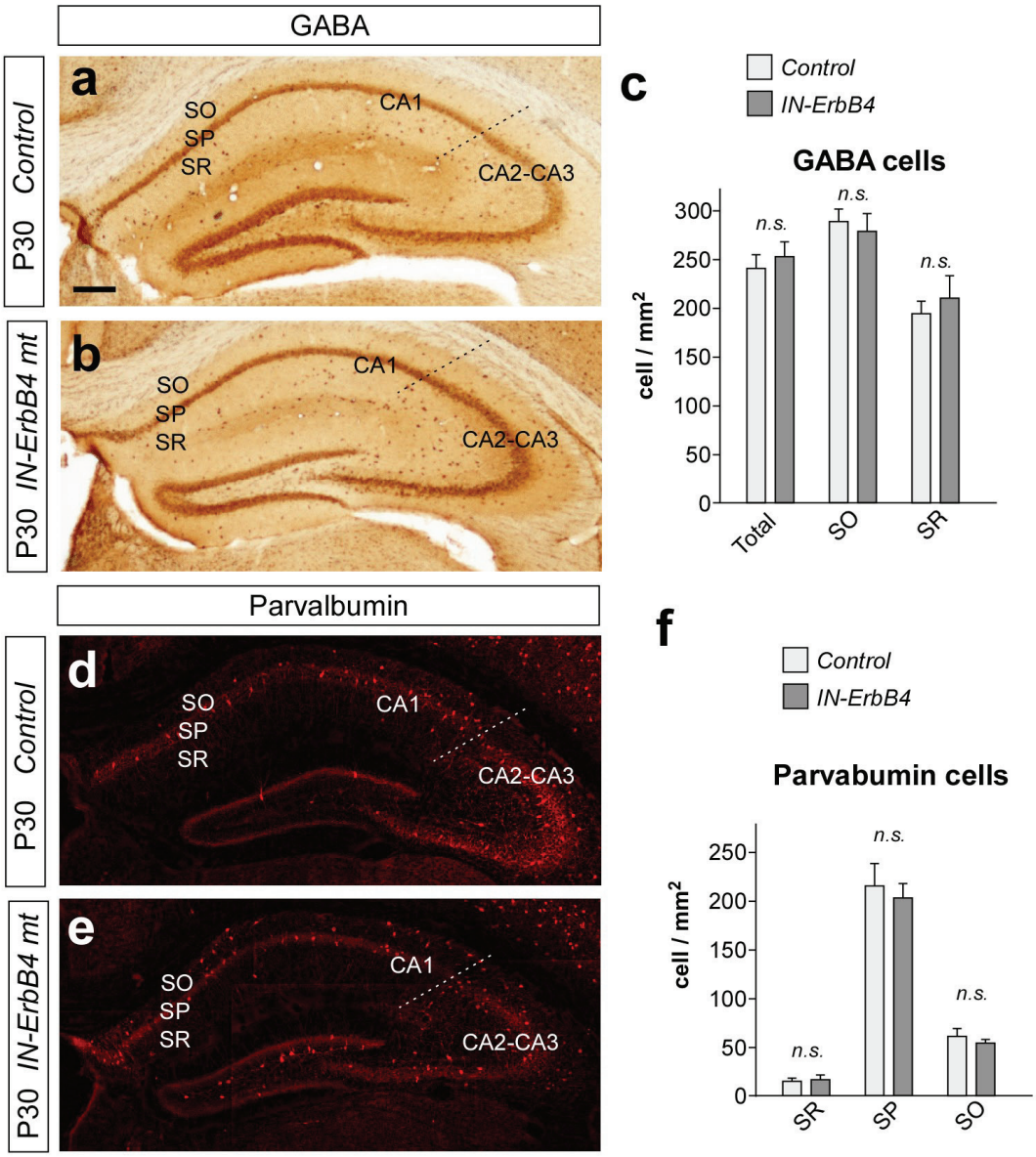

Supplementary Figure 13. Normal numbers of interneurons in the hippocampus of *IN-ErbB4* mutant mice. **a, b, d, e**, Coronal sections through the hippocampus of control and *IN-ErbB4* mutant mice at P30 showing immunohistochemistry against GABA (a, b) and Parvalbumin (d, e). **c, f**, Quantification of the density of interneurons expressing GABA and Parvalbumin in the hippocampus CA1 revealed no differences between both experimental groups. n = 3; GABA: Total, P = 0.62; SO, P = 0.57; SR, P = 0.39. Parvalbumin: SR, P = 0.78; SP, P = 0.64; SO, P = 0.43, χ^2 test. CA1, CA1 region of the hippocampus; CA2-CA3, CA2-CA3 region of the hippocampus; SO, stratum oriens; SP, stratum pyramidale; SR, stratum radiatum. Scale bar: 200 µm.

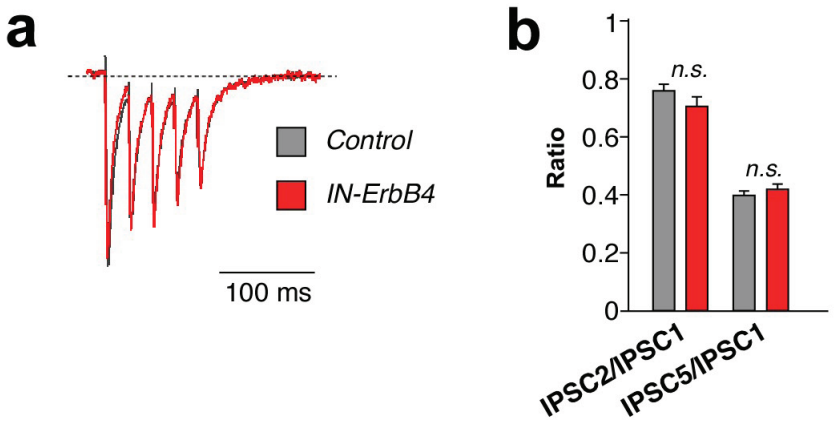

Supplementary Figure 14. Normal GABAergic release in the hippocampus of *IN-ErbB4* mutant mice. **a**, Representative IPSCs induced by a train of stimuli and recorded from control and ErbB4 mutant neurons. **b**, Analysis of pair-pulse ratios (PPRs) revealed no significant differences in the GABAergic vesicles release probability between both experimental groups. n = 6 neurons; IPSC2/IPSC1, P = 0.25; IPSC5/IPSC1, P = 0.19; *t*-test.

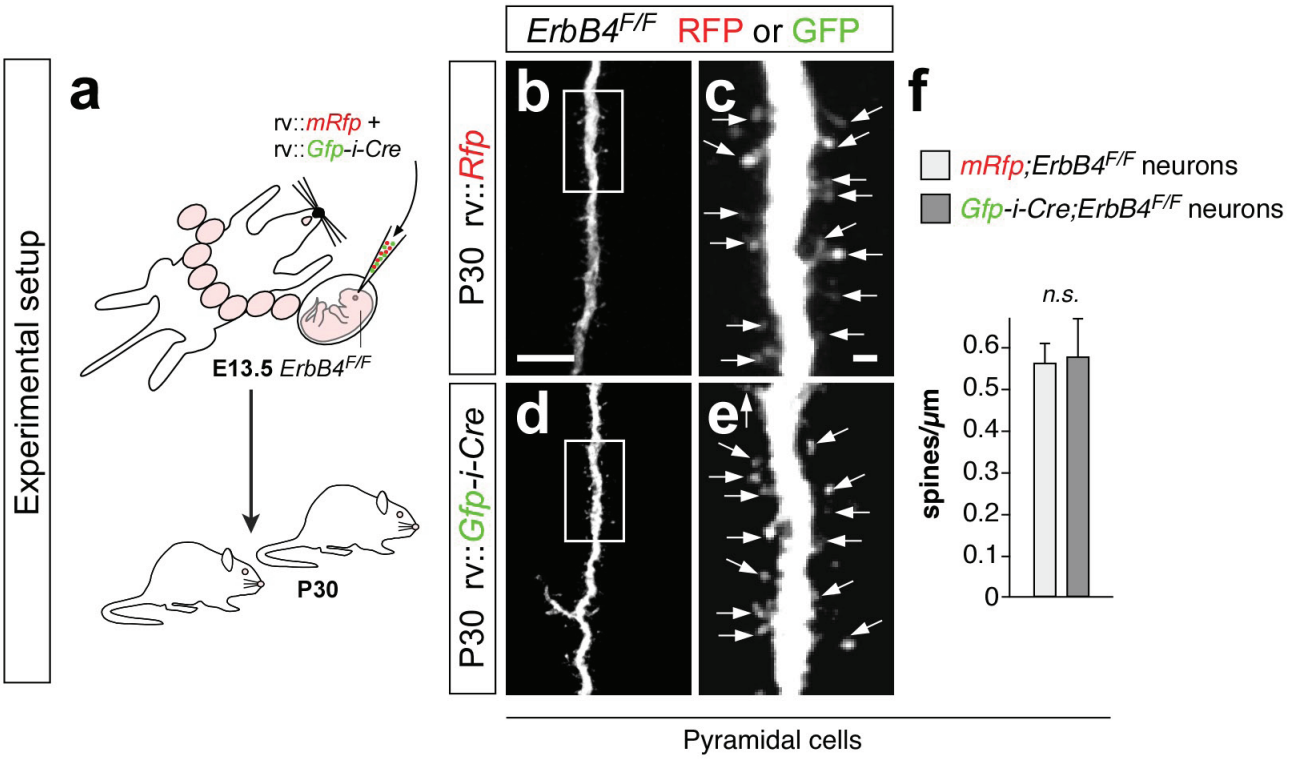

Supplementary Figure 15. Retroviral-mediated deletion of *ErbB4* in pyramidal cells does not alter the density of dendritic spines. **a**, Experimental paradigm. A cocktail of retroviruses (rv) expressing either *mRfp* or *Gfp-i-Cre* was injected in the lateral ventricles of the telencephalon in E13.5 *ErbB4*$^{F/F}$ embryos, and transfected pyramidal cells were analyzed at P30. **b,d**, Representative images of the apical dendrite of control (b) and ErbB4 mutant (d) pyramidal cells. **c,e**, High magnification images of the boxes indicated in (b) and (d), respectively showing the distribution of dendritic spines (arrows) in control (c) and *ErbB4* mutant (e) pyramidal cells. **f**, Quantification of the density of spines revealed no significant differences between both experimental groups. Control: n = 10; *ErbB4* mutant: n = 13 neurons, 2 brains; P = 0.68, *t*-test. Scale bars: 20 µm (b, d), 1 µm (c, e).

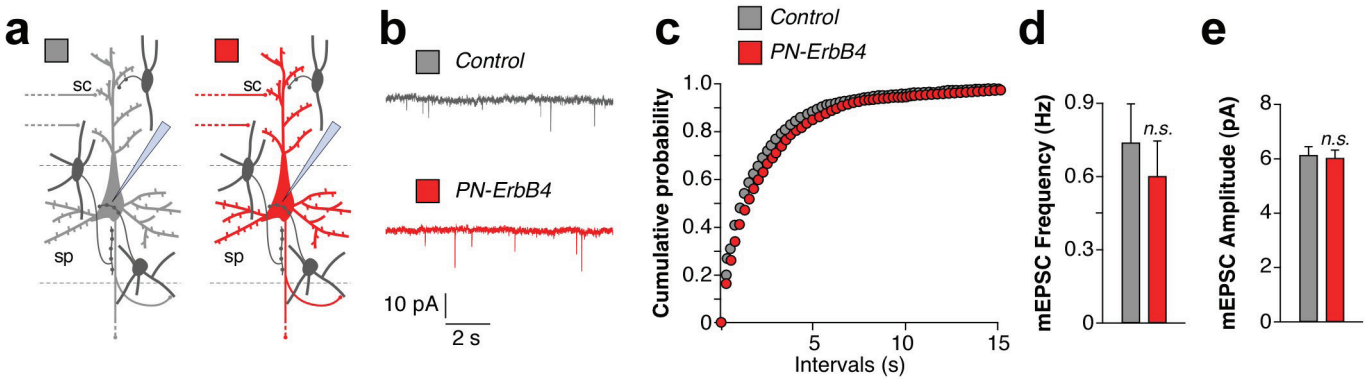

Supplementary Figure 16. Conditional deletion of ErbB4 from pyramidal cells does not disrupt excitatory transmission between them. **a**, Experimental paradigm. mEPSCs were measured from CA1 pyramidal neurons in control and PN-ErbB4 mutant mice at P20. sc, Schaffer collaterals; sp, stratum pyramidale. **b-e**, Representative traces, cumulative plot and measurements of mEPSCs frequencies and amplitudes. Control: n = 22 neurons, 4 brains; *ErbB4* mutant: n = 27 neurons, 4 brains. Frequency, P = 0.23; Amplitude, P = 0.79, *t*-test.

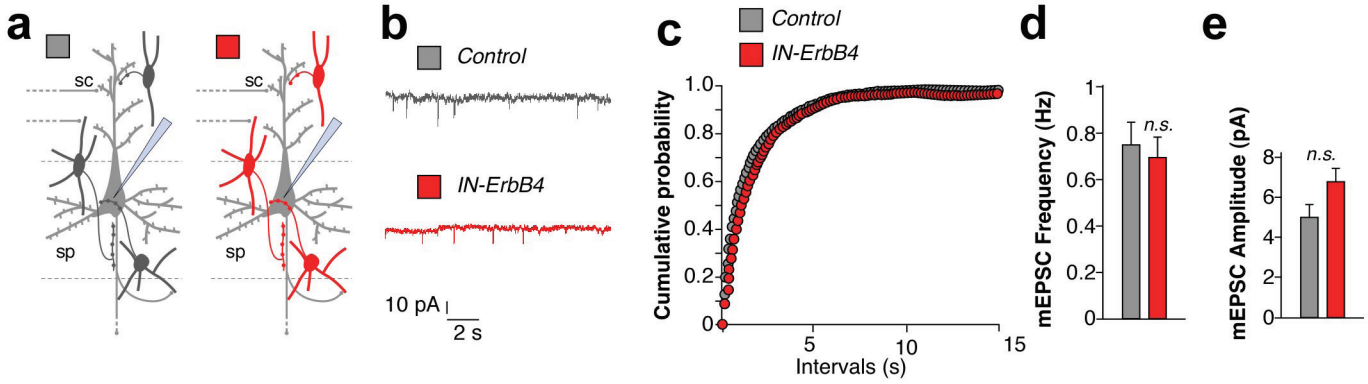

Supplementary Figure 17. Conditional deletion of ErbB4 from interneurons does not disrupt excitatory transmission between pyramidal cells. **a**, Experimental paradigm. mEPSCs were measured from CA1 pyramidal neurons in control and IN-ErbB4 mutant mice at P20. sc, Schaffer collaterals; sp, stratum pyramidale. **b-e**, Representative traces, cumulative plot and measurements of mEPSCs frequencies and amplitudes. Control: n = 6 neurons, 1 brain; *ErbB4* mutant: n = 15 neurons, 3 brains. Frequency, P = 0.74; Amplitude, P = 0.12, *t*-test.